GEOPHYSICS, VOL. 69, NO. 6 (NOVEMBER-DECEMBER 2004); P. 1405–1413, 10 FIGS.
10.1190/1.1836815

Generalized radial inversion of 2D potential field data

João B. C. Silva[1] and Valéria C. F. Barbosa[2]

ABSTRACT

We introduce a new 2D method for inverting potential field data with model constraints designed by the interpreter. Our method uses an interpretation model consisting of a source with polygonal cross-section whose vertices are described by polar coordinates with an origin inside the source. With this coordinate system, constraints in an inversion are easier to develop and apply. Our inversion method assumes a known physical property contrast for the source and estimates the radii associated with the polygon vertices for a fixed number of equally spaced angles from 0° to 360°. A wide variety of constraints may be used to stabilize the solutions by introducing information about the source shape. The method recovers stable solutions whose shapes range from almost circular or pear-shaped to elongated in one or more directions. The convexity constraint applied to the source shape, despite requiring no quantitative information, is more versatile than the other constraints. The convexity constraint efficiently recovers source geometries that are either isometric or elongated in one direction.

INTRODUCTION

Geophysical inversion usually solves for a particular class of physical property distributions in the subsurface. The particular class selected by the interpreter defines the interpretation model. In potential field inversion, the most significant interpretation models used so far may be grouped into one of three categories described below.

The first category comprising early interpretation models consisted of isolated bodies having a simple geometric shape (McGrath and Hood, 1970, 1973; Whitehill, 1973). Despite the strongly restrictive prior information implicitly introduced with the assumption of such interpretation models, the inverse problem of estimating all parameters describing the source position, extension, and physical property is still ill posed because of the ambiguity in simultaneous estimation of the source dimension and physical property (e.g., Whitehill, 1973). This ambiguity can be removed only for models whose geophysical response can be reproduced exactly by equivalent point or line sources such as spheres, cylinders, and thin plates (Gupta, 1983; Abdelrahman and El-Araby, 1993). Because a point or line source has infinitesimal volumes, their dimensions are not estimated. Rather, the unknown parameters in this case are the total excess of mass or dipole moment and the horizontal and vertical coordinates of the source. As a result, the ambiguity involving physical property and volume is not present.

To improve the modeling of real sources, geophysicists used to assume a second category of interpretation model consisting either of (1) vertical, juxtaposed prisms whose only unknown parameters are the prism thicknesses (Cordell and Henderson, 1968; Dyrelius and Vogel, 1972; Pedersen, 1977) or (2) a 2D body defined by a constant polygonal section and whose only unknown parameters are the x- and/or z-coordinates of the polygon vertices (Corbató, 1965; Al-Chalabi, 1972). This additional model complexity led to an inevitable increase in the solution instability, which has not been controlled successfully. Usual procedures to reduce instability include

1) limiting the size of the parameter corrections along the iteration required to solve the nonlinear problem, which favors a solution close to the initial guess so that the prior information used to improve solution stability is concentrated at the initial approximation (Dyrelius and Vogel, 1972; Pedersen, 1977)
2) filtering the data (Corbató, 1965)
3) presuming that several parameters are known (Johnson, 1969; Al-Chalabi, 1971)

Procedures 1 and 3 require strong prior quantitative geological information; therefore, their practical value is limited because most of the available geological information is qualitative and semiquantitative rather than quantitative (Krumbein and Graybill, 1965).

Tikhonov's (1963) regularization method allows introduction of semiquantitative information, but its use was restricted

Manuscript received by the Editor May 20, 2003; revised manuscript received April 12, 2004.
[1]Federal University of Pará–CG, Department of Geophysics, Caixa Postal 1611, Belém, Pará 66017-900, Brazil. Fax: (5591) 211-1693; E-mail: joaobcs@directbr.com.br.
[2]LNCC, Avenue Getúlio Vargas 333, Quitandinha, Petrópolis, Rio de Janeiro 25651-075, Brazil. Fax: (5524) 2231-5595; E-mail: valcris@lncc.br.

outside the former Soviet Union until the English translation was published in 1977 (Tikhonov and Arsenin). Moreover, Tikhonov's regularization is most effective when applied to inverse problems whose unknown parameters represent the same physical entity. It would be meaningless, for example, to stabilize the inversion by minimizing the norm of a parameter vector consisting of the width, thickness, position, and physical property of the source. The only exception is the particular case of a polygon with a known upper (or lower) surface, as in the case of sedimentary basins or the crust–mantle interface. In this case, the depths at prespecified x-coordinates are the parameters to be determined, and the minimum norm or smoothness constraint of the depth to the interface $z(x)$ or of its horizontal derivative can be successfully applied (Chavez and Garland, 1985; Pilkington and Crossley, 1986; Barbosa et al., 1997).

From the 1970s on, a third category of interpretation model began to attract the interest of geophysicists. It consisted of dividing the subsurface region containing the anomalous sources into a number of elementary rectangular homogeneous cells of known size but unknown density. This interpretation model is often claimed by interpreters to permit a more realistic description of real sources. However, it increases tremendously the amount of information demanded by the interpreter and, consequently, the instability of the solutions. This instability can be controlled via Tikhonov's regularization method because all parameters are physical properties. Despite the existence of a variety of stabilizing functionals based on different mathematical formulations, stabilizing functionals effectively reduce the allowable range for the physical property estimate at each cell by imposing a smooth spatial variation (Braile et al., 1974; Bear et al., 1995; Li and Oldenburg, 1998), a homogeneous and compact source (Last and Kubik, 1983; Guillen and Menichetti, 1984; Portniaguine and Zhdanov, 1999), or a combination of these attributes (Acar and Vogel, 1994). As compared to methods assuming homogeneous sources with prespecified geometries, these methods allow more realistic interpretations of homogeneous sources with complex shapes. However, they do not successfully accomplish the task for which they were originally designed: interpreting anomalies produced by sources with arbitrary distributions of physical property. In fact, no method will ever produce such kind of interpretation without introducing a substantial amount of prior information about the source.

In this way, the methods based on the third category of interpretation model resulted in a profound contradiction. On the one hand, the assumed interpretation model allows arbitrary variations; on the other hand, the available constraints necessary to stabilize the solutions impose homogeneous or smoothly varying distributions. Additionally, introducing homogeneity and compactness constraints with this interpretation model is not computationally trivial. Finally, prior information about the source geometry cannot be introduced in a simple and effective way by this interpretation model, resulting in an important limitation because available geological information more properly constrains the source geometry of a homogeneous source than the spatial physical property distribution of an arbitrary source.

We introduce a new potential field inversion method which uses an interpretation model that eliminates most of the difficulties noted above. It consists of a 2D homogeneous source with polygonal cross-section whose number M of vertices and density contrast, together with the coordinates of a point inside the source, are specified by the interpreter. The vertices are described in polar coordinates (r_k, θ_k), and the parameters to be estimated are the radii r_k for fixed values of θ_k given by $2\pi(k-1)/M$. The advantage of our method relative to methods using interpretation models belonging to the three categories described above is that all current stabilizing constraints such as absolute and relative proximity, minimum moment of inertia, and convexity (Silva et al., 2000, 2001a) may be used to incorporate relevant geological information about the source geometry. Methods using interpretation models from the first and second categories cannot incorporate these constraints in an effective way because the parameters to be estimated usually do not represent the same physical entity (a given set of parameters may include density, width, thickness, position, etc.). Methods using interpretation models from the third category may use all of the above-mentioned constraints because all parameters are physical properties, but information about the source geometry can only be introduced indirectly (Last and Kubik, 1983; Guillen and Menichetti, 1984).

THE RADIAL METHOD

In this section we present a nonmathematical overview of the method and the applicable constraints. The mathematical and algorithmic details are given in Appendix A.

Method description

Consider a homogeneous 2D source with arbitrary cross-section S (Figure 1). We approximate the surface S by a simple polygon P with M sides. Instead of describing P by the Cartesian coordinates (x_k, z_k) of its vertices, we describe it by polar coordinates (r_k, θ_k) referred to an arbitrary origin O at $(x_o, z_o) \in S$ with the positive x-axis being the reference direction for the angle θ, considered positive in the clockwise sense. The number of sides M is established by the interpreter on the basis of his conception of the complexity of true source S.

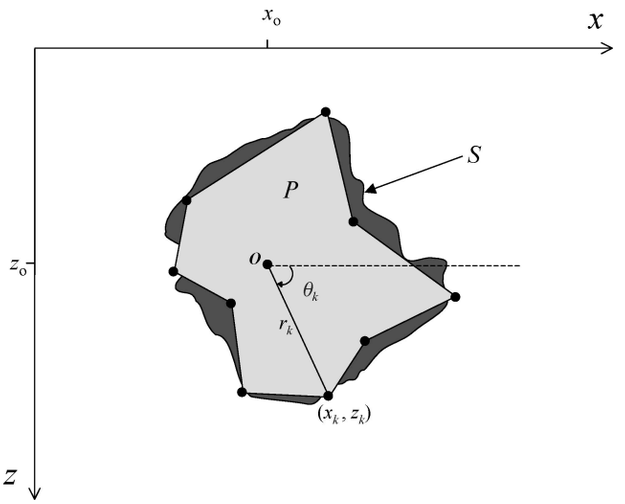

Figure 1. Anomalous source S and interpretation model consisting of a polygon P whose kth vertex is defined by polar coordinates r_k and θ_k.

After establishing the value of M, the angles θ_k are given by $2\pi(k-1)/M, k=1, 2, \ldots, M$.

The forward problem consists of first establishing the origin O and assigning values to the variable M, to $r_k, k=1, 2, \ldots, M$, to the density or susceptibility contrast, and, in the case of a magnetic source, to the inclination and azimuth of the magnetization and geomagnetic field vectors. Then we obtain the gravity or magnetic anomaly using Talwani (1965) and Talwani et al.'s (1959) methods. The inverse problem consists of assigning values to M, to the coordinates of the origin O, to the density or susceptibility contrast, and (for a magnetic source) to the inclination and azimuth of the magnetization and geomagnetic field vectors; then we estimate the values of $r_k, k=1, 2, \ldots, M$ from the observed gravity or magnetic anomaly.

The solution of the unconstrained inverse gravity problem is unique if the density is known and the source belongs to the class of stellar bodies (Novikov, 1938). However, the solution is unstable, and stabilizing constraints must be introduced if a geologically meaningful solution is to be obtained. Because all parameters represent the same physical entity (distances between the center O and the vertices), Tikhonov's regularization method, among others, can be used to introduce any of the currently available constraints (Silva et al., 2000, 2001a), as discussed in the next section.

Even though the assumptions required by our interpretation model are mathematically restrictive, they do not prevent the practical applicability of the method. The premise of a homogeneous source may be (and has been, e.g., Last and Kubik, 1983; Guillen and Menichetti, 1984) successfully used in important interpretation problems involving anomalous igneous bodies and structures such as batholiths, sills, and laccolithic domes. The physical property contrast required by the method is prior geological information that is usually more dependable than the source geometry. The coordinates of the center of mass (or dipole moment of the source) can be estimated in a stable, reliable way for the class of sources that can be expanded into moments up to second order (Medeiros and Silva, 1995a, b). For this class of bodies, which includes the most commonly encountered geologic sources, the center of mass or dipole moment usually lies in the interior of the source.

Possible constraints

The absolute and relative proximity constraints (Silva et al., 2001a) and the constraint describing the concentration of anomalous physical property along preferred directions discussed in this section are incorporated by minimizing the general expression $\tau = \Psi + \Sigma\mu_j\Phi_j, j=1, 2, \ldots, L$, where Ψ is a measure of the data misfit, Φ_j is the functional incorporating the jth constraint, and μ_j is a nonnegative scalar associated with the particular constraint. The inequality and convexity constraints are incorporated in an algorithmic way described below.

Homogeneity and compactness constraints. — These constraints are implicitly introduced by the interpretation model itself. They are strong enough to make the inverse problem solution unique and more stable (shown in the next section) than solutions obtained with the currently used interpretation model consisting of a grid of cells.

Inequality constraint. — This constraint is introduced by transforming the user-defined constrained parameters into unconstrained parameters, computing estimates for them, and returning to the original constrained parameters. It is used mainly to prevent physical absurdities such as negative radii and negative depths to the top.

Absolute proximity constraint on all or a few parameters. — This constraint requires that r_k be close to prespecified values r_k^o, so the functional Φ is given by $\sum_{k=1}^{I}(r_k - r_k^o)^2$, where $I \le M$. Minimizing Φ favors solutions with a specified geometric feature. In particular, if $I = M$ and all r_k^o are constant, the incorporated information is that the source shape is approximately isometric. Nonetheless, even constant r_k^o may, in some cases, produce reliable interpretations of particular elongated sources. If $I < M$, minimizing Φ forces a few r_k to be close to known numerical values $r_k^o, k=1, 2, \ldots, I$, which could be presumed from borehole information. This constraint is used by Berdichevsky and Zhdanov (1984) in interpreting EM data.

Relative proximity constraint on all parameters. — This constraint requires that all parameters be close to each other. It is incorporated by minimizing the functional $\Phi = (r_M - r_1)^2 + \sum_{k=1}^{M-1}(r_{k+1} - r_k)^2$. As in the case of absolute proximity constraint, the incorporated information asserts that the source shape is approximately isometric, even though reliable interpretations of certain elongated sources may be obtained. This kind of constraint is used by Tsirulskiy and Prutkin (1981).

Concentration of anomalous physical property along preferred directions. — This information is introduced by minimizing the functional $\Phi = \sum_{k=1}^{M}(r_k - r_k^o)^2 w_k$, which is a slight modification of the functional used to incorporate absolute proximity constraints. Variables w_k are weights. Small weights are assigned to radii r_k associated with angles θ_k that are close to J specified directions β_j, $j=1, 2, \ldots, J$, along which the source is assumed to extend. This constraint is useful in interpreting complex sources whose preferred orientations are known. The radii associated with angles θ_k, which are far from the preferred directions, are forced to be close to r_k^o.

Convexity. — This attribute is incorporated into the polygon by checking whether r_k is greater than or equal to the distance c_k from the origin O to the intersection of the direction of r_k with the line segment joining the vertices (r_{k-1}, θ_{k-1}) and (r_{k+1}, θ_{k+1}). If it is, then r_k is not changed; otherwise, it is set to c_k. This constraint is versatile, leading to reliable interpretations not only of isometric bodies but also of sources elongated into a single direction. Zhdanov (1973) introduces this constraint using a different mathematical implementation.

EXAMPLES WITH SYNTHETIC GRAVITY DATA

In this section we illustrate the versatility of the proposed method by applying it to three different geological environments. In all tests we introduce inequality constraints (positivity) on the radii and on the depths to the polygon vertices. In addition, all synthetic anomalies are fitted within the simulated

operational errors, and all solutions are stable. The solution stability is inferred by inverting theoretical anomalies corrupted with different pseudorandom noise sequences and verifying if the solutions are close to each other. In all tests where the functional $\tau = \Psi + \Sigma\mu_j\Phi_j$ is minimized, μ_j is the smallest positive value leading to a stable solution.

Laccolithic intrusion

Figure 2 shows the Bouguer anomaly (dots) produced by the simulated laccolithic intrusion shown in Figure 3 (solid line), having a density contrast ρ of 0.4 g/cm^3. The theoretical anomaly was corrupted with zero-mean Gaussian noise with standard deviation of 0.15 mGal. In all tests using this model, we set the origin O at $x_o = 13$ km, $z_o = 1.5$ km, and $\rho = 0.4$ g/cm^3.

Figure 3a shows the inversion result (dashed line) with $M = 8$ and using just positivity constraint on the radii and on the depths to the polygon vertices. Even though the solution is very far from the true source, it is not completely unrealistic; we obtain a rough location and an approximate outline of the true source. If the same anomaly were inverted with the interpretation model consisting of a grid of homogeneous cells and the parameters to be estimated were the cell densities, the result would neither locate nor delineate the true source [see, for example, Silva et al. (2001a), their Figure 6].

Figure 3b shows the result (dashed line) using as a constraint, in addition to positivity, the concentration of mass along the preferred directions ν_1, ν_2, and ν_3. We used $M = 45$, $\mu = 1.2$, and $r_k^o = 0.5$ km for all k. The true source geometry is very well estimated. Figure 3c shows the same test as Figure 3b, except r_k^o is set at 0.75 km for all k. Note that a convex protrusion appears around the origin (black dot). If we choose $r_k^o = 0.25$, a concave depression instead of a convex bulge appears around O, indicating that r_k^o should be selected to minimize either bulges or depressions around O.

The geologically meaningful results produced by Figures 3b and 3c show that the prior information that the anomalous mass is concentrated along three directions is an adequate constraint for this type of geologic setting. To illustrate the consequences of using inadequate constraints to interpret this geological setting, we show inversion examples using constraints of convexity, absolute proximity, or relative proximity. Figures 3d–f show the respective results for the convexity, absolute proximity, and relative proximity constraints on all parameters by setting $M = 45$. For the absolute proximity we used $\mu = 1$ and $r_k^o = 0.5$ km for all k; for the relative proximity constraint, $\mu = 0.5$ was used. All three constraints produce poor results, indicating they are unsuitable for a laccolithic intrusion interpretation because they bias the inversion toward solutions possessing an attribute not displayed by the true source.

To illustrate how information about the source depth originated from a single borehole can significantly improve the overall shape estimate of the source, we repeated the test shown in Figure 3f with the source boundary constrained to be closest to points $x = 18$ km, $z = 1.5$ km and $x = 19$ km, $z = 5.3$ km, with $\mu = 10$ yielding the results in Figures 3g and 3h, respectively. The latter test is just for illustration. Of course, no borehole is expected to extend to depths of 6 km.

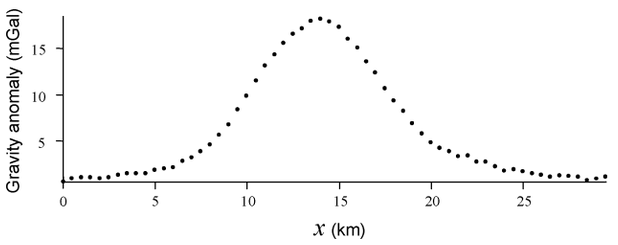

Figure 2. Bouguer anomaly produced by a simulated laccolithic intrusion with density contrast of 0.4 g/cm^3. The theoretical anomaly was corrupted with zero-mean Gaussian noise with a standard deviation of 0.15 mGal.

Faulted salt structure

Figure 4 shows the gravity anomaly (dots) produced by the source shown in Figure 5 (solid line) with $\rho = -0.4$ g/cm^3 and corrupted with zero-mean Gaussian noise with a standard deviation of 0.25 mGal. This model represents a salt structure and

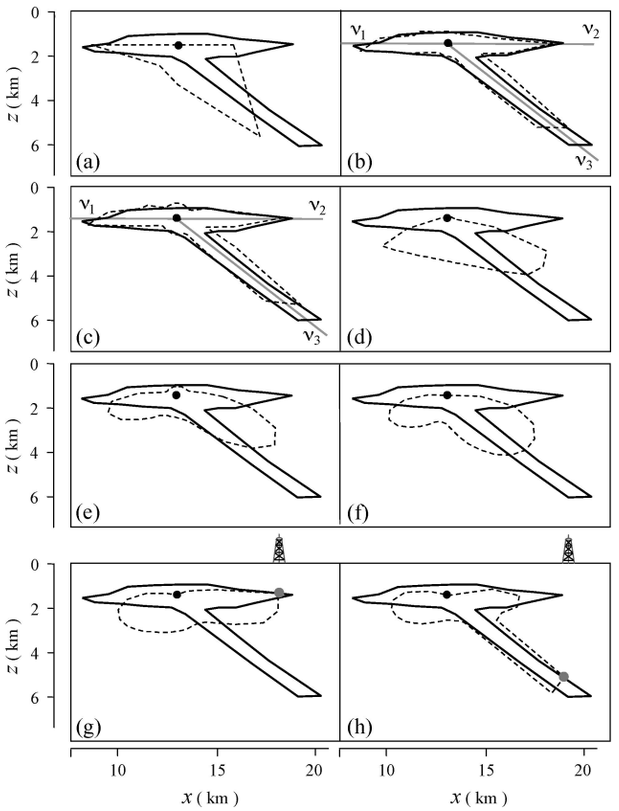

Figure 3. Inversions of the anomaly shown in Figure 2 using the proposed method. In all tests, positivity constraint is incorporated, and the black circle marks point O (x_o, z_o). (a) Using no additional constraint and $M = 8$. (b) Concentrating the anomalous mass along the preferred directions ν_1, ν_2, and ν_3, with $\mu = 1.2$, $r_k^o = 0.5$ km, and $M = 45$. (c) Same as (b) with $r_k^o = 0.75$. (d) Using convexity with $M = 45$. (e) Using an absolute proximity constraint with $\mu = 1$, $r_k^o = 0.5$ km, and $M = 45$. (f) Using a relative proximity constraint with $\mu = 0.5$ and $M = 45$. (g) and (h) Same as (f) but constraining the solution upper boundary by information obtained from a single borehole marked by a gray circle with $\mu = 10$ in both cases.

was inspired by a geological interpretation across the Gypsum Valley, eastern Paradox basin, Colorado (Steenland, 1962). We use $M = 30$, $\rho = -0.4$ g/cm^3, $x_o = 9.5$ km, and $z_o = 3$ km, and we introduce the relative proximity constraint with $\mu = 0.4$ (Figure 5a), the absolute proximity on all parameters with $\mu = 2.0$ and $r_k^o = 1.5$ km for all k (Figure 5b), the absolute proximity on all parameters $\mu = 2.0$ and $r_k^o = 0$ km for all k (Figure 5c), and the convexity constraint (Figure 5d). In Figures 5a and 5b the true source is reasonably delineated because it is roughly isometric and both constraints incorporate this factual property. The test using $r_k^o = 0$ km for all k (Figure 5c) is the minimum Euclidean norm estimator; it produces the worst result because all r_k^o closest to zero is not factual information. The best result consistent with the true source is achieved with the convexity constraint (Figure 5d), which enhances the pear-shaped geometry of the source.

Lens-shaped pluton

Figure 6 shows the gravity anomaly (dots) produced by the source in Figure 7 (solid line) with $\rho = 0.4$ g/cm^3 and corrupted with zero-mean Gaussian noise with a standard deviation of 0.15 mGal. We used $M = 32$, $\rho = 0.4$ g/cm^3, $x_o = 10$ km, and $z_o = 1.5$ km, and we introduced the relative proximity constraint with $\mu = 0.2$ (Figure 7a), the absolute proximity on all parameters with $\mu = 1$ and $r_k^o = 0.5$ km for all k (Figure 7b), the convexity constraint (Figure 7c), and mass concentration along two preferred directions (ν_1 and ν_2, Figure 7d) with $\mu = 1$ and $r_k^o = 0.5$ km for all k. The relative proximity constraint performs poorly in delineating the true source, followed by the absolute proximity constraint which reasonably delineates the source. The best performances are achieved by convexity (Figure 7c) and concentration of mass along preferred directions (Figure 7d).

REAL DATA APPLICATIONS

In all applications in this section, we use positivity constraints on the radii and on the depths to the polygon vertices. In all tests, the estimated solutions are stable and fit acceptably the Bouguer anomaly.

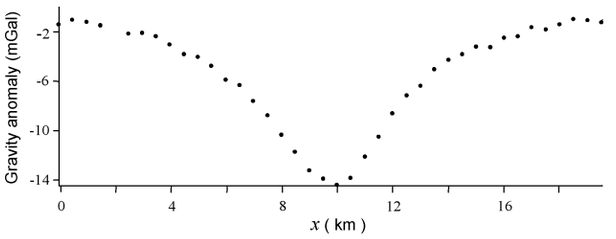

Figure 4. Bouguer anomaly produced by a simulated faulted dome structure intrusion with a density contrast of -0.4 g/cm^3. The theoretical anomaly is corrupted with zero-mean Gaussian noise with a standard deviation of 0.25 mGal.

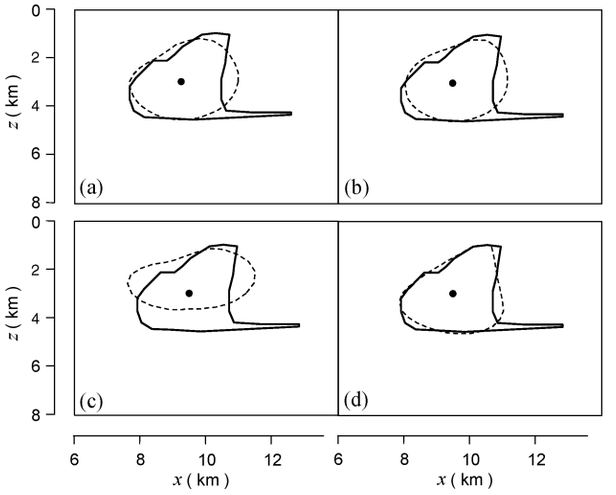

Figure 5. Inversions of the anomaly shown in Figure 4 using the proposed method. In all tests, a positivity constraint is incorporated, $M = 30$ is used, and the black circle marks point O (x_o, z_o). (a) Using a relative proximity constraint with $\mu = 0.4$. (b) and (c) Using an absolute proximity constraint with $\mu = 2$, $r_k^o = 1.5$ km, and $\mu = 2.0$, $r_k^o = 0$ km, respectively. (d) Using a convexity constraint.

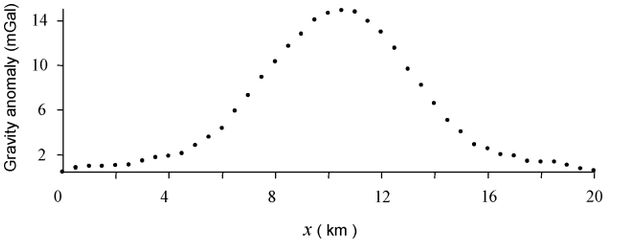

Figure 6. Bouguer anomaly produced by a simulated lens-shaped pluton with a density contrast of 0.4 g/cm^3. The theoretical anomaly was corrupted with zero-mean Gaussian noise with a standard deviation of 0.15 mGal.

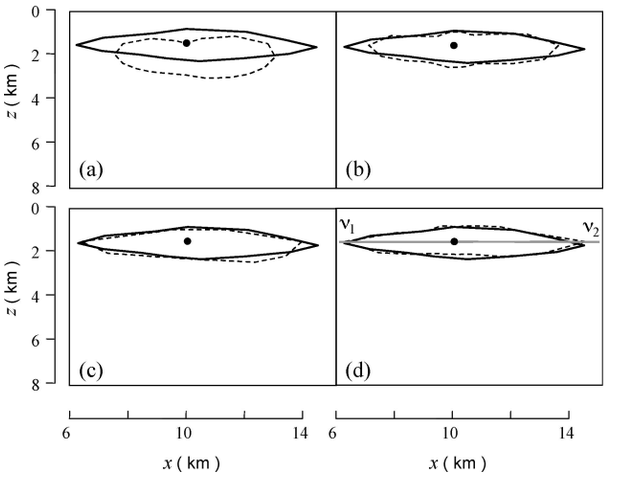

Figure 7. Inversions of the anomaly shown in Figure 6 using the proposed method. In all tests, a positivity constraint is incorporated, $M = 32$ is used, and the black circle marks point O (x_o, z_o). (a) Using a relative proximity constraint with $\mu = 0.2$. (b) Using an absolute proximity constraint with $\mu = 1$, $r_k^o = 0.5$ km. (c) Using a convexity constraint. (d) Concentrating the anomalous mass along directions ν_1 and ν_2 with $\mu = 1$ and $r_k^o = 0.5$ km.

Humble Dome

Figure 8a shows an east–west profile passing through the center of the Humble Dome Bouguer anomaly (Nettleton, 1976). This anomaly (dots) has been interpreted by presuming a fixed spherical shape and a known density contrast (Nettleton, 1976; Abdelrahman and El-Araby, 1993). We adapt our method to introduce information about the source extension D_y along the y-direction—that is, by assuming that the source is 2.5D. We assume that $\rho = -0.3$ g/cm^3, $M = 31$, $D_y = 3.5$ km, $x_o = 11.2$ km, and $z_o = 4.5$ km. The results are shown in Figure 8b using (1) the relative proximity constraint with $\mu = 0.75$ (solid line) and (2) a combination of convexity and relative proximity constraints with $\mu = 0.01$ (dashed line). Constraint (1) produces a roughly isometric source as imposed a priori in previous interpretations, whereas the combination of constraints (2) produces an alternative interpretation: an elongated source dipping to the east. Both solutions are stable. The fitted anomalies are shown in Figure 8a.

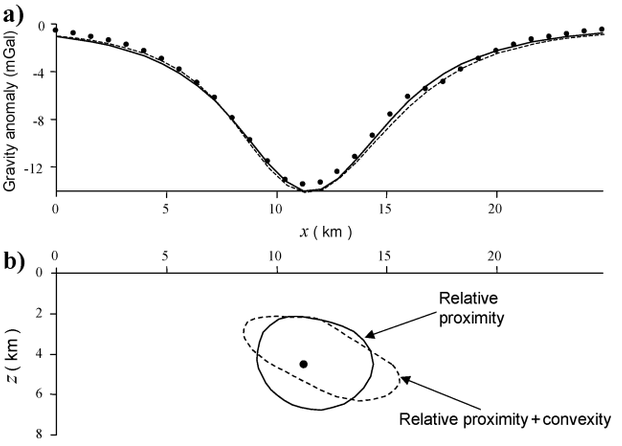

Figure 8. Bouguer anomaly over Humble Dome (dots). (b) Inversions using a positivity constraint, assuming $\rho = -0.3$ g/cm^3 and $M = 31$. The solid line is the solution using a relative proximity constraint with $\mu = 0.75$. The dashed line is the solution using a combination of convexity and relative proximity constraints with $\mu = 0.01$. The fitted anomalies are shown in (a). The black circle in (b) marks point O (x_o, z_o).

Castelsarrasin granitic body

Figure 9a shows the Bouguer anomaly (dots) produced by the granitic body of Castelsarrasin in the Aquitaine basin, France (Guillen and Menichetti, 1984). A drill hole hit the uppermost part of the granitic body at a depth of 500 m (Guillen and Menichetti, 1984). Density contrasts smaller than -0.15 g/cm^3 were considered acceptable by Guillen and Menichetti (1984).

We apply our method to this anomaly assuming a 2D source, $\rho = -0.2$ g/cm^3, $M = 55$, $x_o = 10$ km, and $z_o = 4$ km. The inversion result using a convexity constraint (solid line, Figure 9b) shows a preferred orientation that coincides with previous interpretations using explicit prior information about preferred directions of mass concentration (Guillen and Menichetti, 1984).

From the inversion result using just convexity and positivity constraints (solid line, Figure 9b), we define the preferred directions ν_1 and ν_2. A second inversion result (dashed line, Figure 9b) using the combination of concentration of mass along preferred directions ν_1 and ν_2 (with $\mu = 1$ and $r_k^o = 1.5$ km for all k) and convexity constraints shows an estimated source slightly longer and thinner than the interpretation using just convexity and positivity (solid line, Figure 9a). The fitted anomalies are shown in Figure 9a.

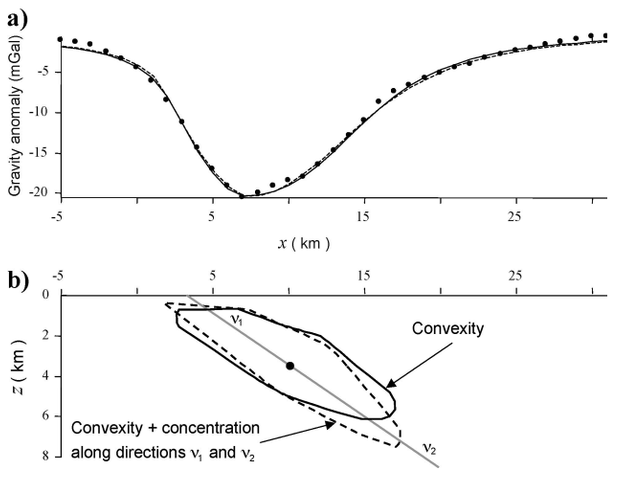

Figure 9. (a) Bouguer anomaly over the Castelsarrasin granitic intrusion (dots). (b) Inversions using a positivity constraint, assuming $\rho = -0.2$ g/cm^3 and $M = 55$. The solid line is the solution using a convexity constraint. The dashed line is the solution using a combination of concentration of mass along preferred directions ν_1 and ν_2 with $\mu = 1$ and $r_k^o = 1.5$ km and convexity constraints. The fitted anomalies are shown in (a). The black circle in (b) marks point O (x_o, z_o).

CONCLUSIONS

We have presented a new 2D potential field inversion method that uses an interpretation model consisting of sources with polygonal cross sections whose vertices are described by polar instead of Cartesian coordinates. We assume a fixed number of equally spaced angles from 0° to 360°, defined according to the assigned number of sides to the polygon. The physical property contrast is presumed constant and known, so all unknown parameters are the distances from an arbitrary point (located inside the source) to the polygon vertices. As a result, any constraint imposed on the parameters may incorporate prior information on the source geometry. In this way, all available types of constraints may be used to find stable and geologically meaningful solutions. Although these constraints have been used individually in previous methods, our method can use all available constraints either individually or in a combined way.

We illustrate the versatility of the method with synthetic and real data by applying it to gravity anomalies from different geological settings. In the case of isometric sources, the relative proximity and convexity constraints produce very good results without requiring quantitative prior information about the source extent. On the contrary, the absolute proximity constraint requires prior information. For a source elongated along a single direction, the relative proximity constraint has

poor performance whereas the absolute proximity constraint may produce a good result if the smallest dimension of the source is known or estimated. The concentration of a physical property along a preferred direction presents the best results but requires prior information about this direction. On the other hand, the convexity constraint has very good performance without prior knowledge about the source dimension and preferred direction. In complex geological environments with sources elongated in more than one direction, the concentration of a physical property along preferred directions is the only constraint that produces good results, but it requires a lot of prior geological information. Borehole information about the depth to the source top may substantially improve the geological validity of the solution when incorporated with other constraints based on factual geological information about the source geometry.

Although the presented implementation of the radial method considers only a single 2D homogeneous source, it can be extended to multiple 3D sources with no conceptual difficulties. The computational effort, however, may be high. The method can also be extended to inhomogeneous sources as long as an analytic expression is available for the gravity or magnetic field produced by a source whose physical property varies according to a specified law. For example, analytic expressions for the gravity anomaly produced by sources whose density contrast decrease with depth according to a linear, hyperbolic, or parabolic law are presently available and can be incorporated in the radial method if the geologic setting requires. Our method may additionally be extended to invert magnetotelluric, EM, and seismic data. Finally, combinations of constraints may be used to obtain solutions with more complex shapes warranted by the geological information.

APPENDIX A

MATHEMATICAL AND ALGORITHMIC DETAILS

Consider a 2D source with a polygonal cross-section defined by the radii r_k and angles $\theta_k = 2\pi(k-1)/M$, $k = 1, 2, \ldots, M$ about the origin O at (x_o, z_o) (Figure 1). The gravity and magnetic anomaly $f(\mathbf{r})$ produced by such a source may be computed, respectively, by Talwani et al.'s (1959) and Talwani's (1965) methods, where $\mathbf{r}$ is the M-dimensional vector containing the radii r_k. The unconstrained inverse problem consists of estimating $\mathbf{r}$ from a set of N observations $\mathbf{y}$ by minimizing

$$\Psi(\mathbf{r}) = \|\mathbf{y} - f(\mathbf{r})\|^2, \tag{A-1}$$

where $\|\cdot\|$ is the Euclidean norm. To introduce the relative proximity, absolute proximity, and concentration of a physical property along preferred directions, we define the stabilizing functionals

$$\Phi_1(\mathbf{r}) = \|\mathbf{B}\mathbf{r}\|^2 \tag{A-2}$$

and

$$\Phi_2(\mathbf{r}) = \|\mathbf{W}(\mathbf{r} - \mathbf{r}^{\mathbf{o}})\|^2, \tag{A-3}$$

where $\mathbf{B}$ is an $M \times M$ first difference discrete matrix operator (Barbosa et al., 1997) of the form

$$\begin{bmatrix} 1 & -1 & 0 & \cdots & 0 & 0 \\ 0 & 1 & -1 & \cdots & 0 & 0 \\ \vdots & \vdots & \vdots & \cdots & \vdots & \vdots \\ 0 & 0 & 0 & \cdots & 1 & -1 \\ -1 & 0 & 0 & \cdots & 0 & 1 \end{bmatrix},$$

$\mathbf{r}^{\mathbf{o}}$ is a reference parameter vector, and $\mathbf{W}$ is a diagonal weighting matrix. To incorporate relative proximity, we minimize Φ_1. To incorporate absolute proximity and concentration of physical property along preferred directions, we minimize Φ_2 in the following way. To incorporate absolute proximity constraint, we set $\mathbf{W}$ to the identity matrix. To impose a concentration of the physical property along J preferred directions β_j, $j = 1, \ldots, J$, we define the kth diagonal element of $\mathbf{W}$ by

$$w_{kk} = \min_j \{|\sin[0.5(\beta_j - \theta_k)]| + \varepsilon\}^2, \tag{A-4}$$

where ε is a small positive number related to the assumed ratio p between the smallest and largest dimensions of the source. Because the maximum weight is one, ε should be close to p.

To incorporate borehole information about the source depth to the top, we proceed in the following way. Let the depth to the source top be known at points $Q_i(r_i, \theta_i\}, i = 1, 2, \ldots, I$. We determine the index $k(i)$ such that $\theta_{k(i)} < \theta_i < \theta_{k(i)+1}$, where $\theta_{k(i)}$ and $\theta_{k(i)+1}$ are the angles defining the source top ($\pi < \theta_{k(i)} < 2\pi$ and $\pi < \theta_{k(i)+1} < 2\pi$) and are associated with the kth polygon vertex which is closest to θ_i. Next, we find the projections $b_{i,k(i)}$ and $b_{i,k(i)+1}$ of Q_i on the straight lines coinciding with the directions of $r_{k(i)}$ and $r_{k(i)+1}$. The lengths of $r_{k(i)}$ and $r_{k(i)+1}$ are then forced to be closest to projections $b_{i,k(i)}$ and $b_{i,k(i)+1}$ by minimizing the functional

$$\Phi_3 = \sum_{i=1}^{I} (r_{k(i)} - b_{i,k(i)})^2 + (r_{k(i)+1} - b_{i,k(i)+1})^2. \tag{A-5}$$

All of the above constraints are introduced into the unconstrained problem of minimizing functional A-1 by minimizing

$$\tau = \|\mathbf{y} - f(\mathbf{r})\|^2 + \mu_1\|\mathbf{B}\mathbf{r}\|^2 + \mu_2\|\mathbf{W}(\mathbf{r} - \mathbf{r}^{\mathbf{o}})\|^2 + \mu_3 \sum_{i=1}^{I} (r_{k(i)} - b_{i,k(i)})^2 + (r_{k(i)+1} - b_{i,k(i)+1})^2, \tag{A-6}$$

where μ_1, μ_2, and μ_3 are nonnegative scalars. Because borehole information is usually more reliable than other prior information, μ_3 is usually much greater than μ_1 and μ_2.

The inequality and convexity constraints are introduced algorithmically and are described later.

Functional A-6 is nonlinear in $\mathbf{r}$ and is minimized via Newton's method with

$$\Delta\mathbf{r}_i = -\{H[\Psi(\mathbf{r}) + \Phi_1(\mathbf{r}) + \Phi_2(\mathbf{r})]\}^{-1} G[\Psi(\mathbf{r}) + \Phi_1(\mathbf{r}) + \Phi_2(\mathbf{r})] \tag{A-7}$$

at the ith iteration, where $H(\cdot)$ and $G(\cdot)$ are, respectively, the Hessian and the gradient operators. The Gauss-Newton

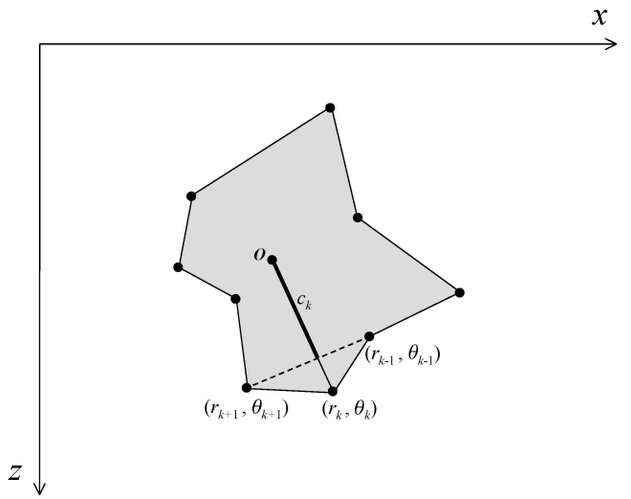

Figure A-1. Criterion used in incorporating the convexity constraint. At any iteration, if the estimate of radius r_k is greater or equal to the line segment c_k, the estimate is unchanged; otherwise, it is set to c_k.

approximation of $H[\Psi(\mathbf{r})]$ and the Marquardt modification of Newton's step (Silva et al., 2001b) are used.

The inequality constraints used in the present method prevent the radii from becoming smaller than zero and greater than geological or physical limits defining the vector $\mathbf{r}_{\max}$. These constraints are expressed as

$$\mathbf{0} < \mathbf{r} < \mathbf{r}_{\max}, \tag{A-8}$$

where $\mathbf{0}$ is the null vector and the inequality sign is applied element by element. The kth element of vector $\mathbf{r}_{\max}$ is given either by

$$r_{\max_k} = q, \qquad 0 \le \theta_k \le \pi, \tag{A-9}$$

where q is a very large positive number, or by

$$r_{\max_k} = \frac{z_o}{\text{abs}[\sin(\theta_k)]}, \qquad \pi < \theta_k < 2\pi. \tag{A-10}$$

Condition A-9 establishes a limit for the source base, whereas condition $(A-10)$ prevents the z-coordinates of the polygon vertices from becoming negative. The inequality constraints A-8 are incorporated in three steps. The first is transforming the original parameter vector $\mathbf{r} \equiv \{r_k\}$, $\in (0, r_{\max_k})$, $k = 1, 2, \ldots, M$ into the unconstrained parameter vector $\mathbf{r}^* \equiv \{r_k^*\} \in (-\infty, +\infty)$, $k = 1, \ldots, M$ by the homeomorphic transformation

$$r_k^* = -\ln \frac{r_{\max_k} - r_k}{r_k}. \tag{A-11}$$

Step two is computing $\Delta\mathbf{r}^* = \mathbf{T}\Delta\mathbf{r}$ at each iteration with equation A-7, where $\mathbf{T}$ is an $M \times M$ matrix whose jth element is $r_k - (r_k^2/r_{\max_k})$, and summing it with the estimate $\mathbf{r}^*$ given at the current iteration. The final step is returning to the original parameter vector $\mathbf{r}$ using the inverse transformation:

$$r_k = \frac{r_{\max_k}}{1 + \exp(-r_k^*)}. \tag{A-12}$$

The convexity constraint is introduced algorithmically by checking at each iteration the inequality $r_k \ge c_k$, $k = 1, 2, \ldots, M$, where c_k is the distance from the center O to the intersection of the direction of r_k with the line segment joining the vertices (r_{k-1}, θ_{k-1}) and (r_{k+1}, θ_{k+1}) (Figure A-1). If the inequality holds, the estimate of r_k at the current iteration is unchanged; otherwise, it is set to c_k.

ACKNOWLEDGMENTS

We are grateful to associate editor D. Ravat, assistant editor Yonghe Sun, and two anonymous reviewers for their careful revision and constructive criticism. The authors were supported in this research by PCI-LNCC\MCT and Conselho Nacional de Desenvolvimento Científico e Tecnológico (CNPq), Brazil. V. C. F. B. was also supported by CNPq under contract 472229/03-6 and by FAPERJ (Programa Primeiros Projetos, Edital MCT/CNPq/CT-INFRA/FAPERJ No. 05/2003).

REFERENCES

Abdelrahman, E. M., and T. M. El-Araby, 1993, A least-squares minimization approach to depth determination from moving average residual gravity anomalies: Geophysics, **59**, 1779–1784.

Acar, R., and C. R. Vogel, 1994, Analysis of total variation penalty methods: Inverse Problems, **10,** 1217–1229.

Al-Chalabi, M., 1971, Some studies relating to nonuniqueness in gravity and magnetic inverse problems: Geophysics, **36**, 835–855.

——— 1972, Interpretation of gravity anomalies by nonlinear optimization: Geophysical Prospecting, **20**, 1-16.

Barbosa, V. C. F., J. B. C. Silva, and W. E. Medeiros, 1997, Gravity inversion of basement relief using approximate equality constraints on depths: Geophysics, **62**, 1745–1757.

Bear, G. W., H. J. Al-Shukri, and A. J. Rudman, 1995, Linear inversion of gravity data for 3-D density distributions: Geophysics, **60**, 1354–1364.

Berdichevsky, M. N., and M. S. Zhdanov, 1984, Advanced theory of deep geomagnetic soundings: Elsevier Science Publishing Company, Inc.

Braile, L. W., G. R. Keller, and W. J. Peeples, 1974, Inversion of gravity data for two-dimensional density distributions: Journal of Geophysical Research, **79**, 2017–2021.

Chavez, R. E., and G. D. Garland, 1985, Linear inversion of gravity data using the spectral expansion method: Geophysics, **50**, 820–824.

Corbató, C. E., 1965, A least-squares procedure for gravity interpretation: Geophysics, **30**, 228–233.

Cordell, L., and R. G. Henderson, 1968, Iterative three-dimensional solution of gravity anomaly data using a digital computer: Geophysics, **33**, 596–601.

Dyrelius, D., and A. Vogel, 1972, Improvement of convergence in iterative gravity interpretation: Geophysical Journal, Royal Astronomical Society, **27**, 195–205.

Guillen, A., and V. Menichetti, 1984, Gravity and magnetic inversion with minimization of a specific functional: Geophysics, **49**, 1354–1360.

Gupta, O. P., 1983, A least-squares approach to depth determination from gravity data: Geophysics, **48**, 357–360.

Johnson, W. W., 1969, A least-squares method of interpreting magnetic anomalies caused by two-dimensional structures: Geophysics, **34**, 65–74.

Krumbein, W. C., and F. A. Graybill, 1965, An introduction to statistical methods in geology: McGraw-Hill Book Company.

Last, B. J., and K. Kubik, 1983, Compact gravity inversion: Geophysics, **48**, 713–721.

Li, Y, and D. W. Oldenburg, 1998, 3-D inversion of gravity data: Geophysics, **63**, 109–119.

McGrath, P. H., and P. J. Hood, 1970, The dipping dike case: A computer curve-matching method of magnetic interpretation: Geophysics, **35**, 831–848.

——— 1973, An automatic least-squares multimodel method for magnetic interpretation: Geophysics, **38**, 349–358.

Medeiros, W. E., and J. B. C. Silva, 1995a, Gravity source moment inversion: A versatile approach to characterize position and 3-D orientation of anomalous bodies: Geophysics, **60**, 1342–1353.

——— 1995b, Simultaneous estimation of total magnetization direction and 3-D spatial orientation: Geophysics, **60**, 1365–1377.

Nettleton, L. L., 1976, Gravity and magnetics in oil prospecting: McGraw-Hill Book Company.

Novikov, P. S., 1938, Uniqueness of the solution of the inverse problem of potential theory (in Russian): Bulletin of the Academy of Science, USSR, **18**, 165–168.
Pedersen, L. B., 1977, Interpretation of potential field data—A generalized inverse approach: Geophysical Prospecting, **25**, 199–230.
Pilkington, M., and D. J. Crossley, 1986, Determination of crustal interface topography from potential fields: Geophysics, **51**, 1277–1284.
Portniaguine, O., and M. S. Zhdanov, 1999, Focusing geophysical inversion images: Geophysics, **64**, 874–887.
Silva, J. B. C., W. E. Medeiros, and V. C. F. Barbosa, 2000, Gravity inversion using convexity constraint: Geophysics, **65**, 102–112.
——— 2001a, Potential field inversion: Choosing the appropriate technique to solve a geologic problem: Geophysics, **66**, 511–520.
——— 2001b, Pitfalls in nonlinear inversion: Pure and Applied Geophysics, **158**, 945–964.
Steenland, N. C., 1962, Gravity and aeromagnetic exploration in the Paradox basin: Geophysics, **27**, 73–89.
Talwani, M., 1965, Computation with the help of a digital computer of magnetic anomalies caused by bodies of arbitrary shape: Geophysics, **30**, 797–817.
Talwani, M., J. C. Worzel, and M. Landisman, 1959, Rapid gravity calculations for two-dimensional bodies with application to the Mendocino submarine fracture zone: Journal of Geophysical Research **64**, 49–59.
Tikhonov, A. N., 1963, Regularization of ill-posed problems (in Russian): Doklady Akadyemii Nauk, **153**, 49–52 .
Tikhonov, A. N., and V. Y. Arsenin, 1977, Solutions of ill-posed problems: V. H. Winston & Sons.
Tsirulskiy, A. V., and I. L. Prutkin, 1981, On the solution of the inverse problem of gravimetry for arbitrary classes of two-dimensional and three-dimensional potentials, I: Academy of Science, USSR. Physics of the Solid Earth, **17**, 836–841.
Whitehill, D. E., 1973, Automated interpretation of magnetic anomalies using the vertical prism model: Geophysics, **38**, 1070–1087.
Zhdanov, M. S., 1973, Determination of the boundary of the convex body from the gravity potential (in Russian): Applied Geophysics, **72**, 142–153 .